





OPEN

Understanding vegetation phenology responses to easily ignored climate factors in china's mid-high latitudes

Qianfeng Wang^{1,3}, Huixia Chen¹, Feng Xu¹, Virgilio A. Bento², Rongrong Zhang¹, Xiaoping Wu¹ & Pengcheng Guo^{4,5}

Previous studies have primarily focused on the influence of temperature and precipitation on phenology. It is unclear if the easily ignored climate factors with drivers of vegetation growth can effect on vegetation phenology. In this research, we conducted an analysis of the start (SOS) and end (EOS) of the growing seasons in the northern region of China above 30°N from 1982 to 2014, focusing on two-season vegetation phenology. We examined the response of vegetation phenology of different vegetation types to pre-season climatic factors, including relative humidity (RH), shortwave radiation (SR), maximum temperature (Tmax), and minimum temperature (Tmin). Our findings reveal that the optimal pre-season influencing vegetation phenology length fell within the range of 0–60 days in most areas. Specifically, SOS exhibited a significant negative correlation with Tmax and Tmin in 44.15% and 42.25% of the areas, respectively, while EOS displayed a significant negative correlation with SR in 49.03% of the areas. Additionally, we identified that RH emerged as the dominant climatic factor influencing the phenology of savanna (SA), whereas temperature strongly controlled the SOS of deciduous needleleaf forest (DNF) and deciduous broadleaf forest (DBF). Meanwhile, the EOS of DNF was primarily influenced by Tmax. In conclusion, this study provides valuable insights into how various vegetation types adapt to climate change, offering a scientific basis for implementing effective vegetation adaptation measures.

Keywords Phenology, Vegetation, Pre-season, Climate change

Vegetation phenology, denoting the recurrent seasonal fluctuations in vegetation growth, constitutes a crucial indicator of vegetation development with profound implications for terrestrial carbon balance and ecosystem productivity^{1–5}. As an exceptionally responsive bio-indicator, vegetation phenology is a particularly important asset to climate change, making it an invaluable tool for monitoring ecological responses to shifting climate conditions^{3,6–8}. Over recent decades, the dynamics of vegetation phenology have garnered global attention, highlighting the intricate interplay between phenology and climatic factors^{2,9,10}. Consequently, comprehensive investigations into ecosystem responses to climate variables are essential for deepening our comprehension of vegetation dynamics within the context of climate change¹¹.

The influence of climate change on phenology has emerged as a focal point in vegetation phenology research. Uncertainty about future climate change is growing^{12–15}. Previous studies have explored the effect of temperature and precipitation on vegetation phenology^{4,16,17}. However, it is crucial to acknowledge that external climatic drivers affecting vegetation phenology encompass not only temperature and precipitation but also factors such as relative humidity, solar radiation, maximum and minimum temperatures. These variables engage in complex interactions that either facilitate or constrain natural vegetation growth^{13,17–21}. While temperature's primary role in influencing vegetation phenology is widely recognized, the distinct impacts of relative humidity and solar radiation remain less clear^{3,22–24}. Notably, relative humidity significantly influences nutrient phenology in

¹College of Environmental and Safety Engineering/The Academy of Digital China (Fujian), Fuzhou University, Fuzhou 350116, China. ²Faculdade de Ciências, Instituto Dom Luiz, Universidade de Lisboa, 1749-016 Lisboa, Portugal. ³Key Lab of Spatial Data Mining & Information Sharing, Ministry of Education of China, Fuzhou 350116, China. ⁴School of Ecology and Environment, Hainan University, Haikou 570228, China. ⁵Hainan Guowei Eco Environmental Co., Ltd, Haikou 570203, China. ✉email: wangqianfeng@fzu.edu.cn; guopengcheng08@mails.ucas.ac.cn

specific vegetation types^{25,26}, while solar radiation, specifically shortwave radiation, exerts considerable influence by modulating photosynthetically active radiation. Some studies suggest that increased photosynthetically active radiation advances leaf emergence and retards leaf senescence^{27,28}. Additionally, while temperature is acknowledged as the primary driver of vegetation phenology, many studies have proposed asymmetric effects of maximum and minimum temperatures on phenological patterns^{29–31}. Furthermore, various vegetation types exhibit diverse responses to climatic elements, contributing to spatial heterogeneity both between and within regions^{32–35}. In sum, examining the influence of these neglected climatic factors on phenology across different vegetation types is imperative.

Remote sensing identification of vegetation phenology is mostly based on seasonal changes in vegetation indices. Despite the emergence of various vegetation indices, the Normalized Differences Vegetation Index (NDVI) remains a cornerstone in vegetation phenology research due to its global acceptance, simplicity, and efficacy^{36,37}. In addition, the initial remotely sensed vegetation indices need smoothing and noise reduction due to their inherent variability³⁸. Among the various smoothing methods, the empirical method is the simplest to apply, but it is usually sensitive to empirical parameters such as noise threshold and synthesis cycle length³⁹. Although the data conversion method is more flexible in capturing high-frequency changes in the curves, it has poor smoothing ability and relies too much on ground-based phenology data^{40,41}. The curve-fitting method, on the other hand, uses a mathematical function to estimate the time-series trajectory of vegetation growth without the need to set empirical thresholds in advance, which is relatively more objective⁴². Among them, the Savitzky-Golay filter can maximize the retention of data information while eliminating noise interference, which makes it particularly well-suited for extracting climate-related insights from different vegetation^{43,44}. Commonly used methods for determining key phenological parameters include the threshold method and the method for detecting changes in vegetation indices. The threshold method is widely used in vegetation phenology extraction because of its simple calculation method. However, it is sensitive to noise, has poor robustness, and is not suitable for climate studies in different regions and vegetation types^{45,46}. The change detection method extracts candidate parameters by directly detecting the change characteristics of the vegetation index time series curves³⁶. In contrast, the change monitoring method is widely used and can effectively determine key parameters of vegetation phenology⁴⁷. Partial vegetation, especially crops, undergoes two growing seasons due to natural environmental factors such as climate and soil. However, existing research focuses more on single growing season vegetation, leaving a gap in the study of phenology in two-season vegetation. There remains significant uncertainty regarding the extraction of phenological parameters in dual-season vegetation and their response mechanisms to pre-season climate factors. Meanwhile, the accuracy of the parameters needs to be improved due to the lack of ground data calibration^{48,49}. Therefore, this study was calibrated with ground-based phenology data to consider two-seasonal vegetation phenology parameters and to extract phenology parameters for different vegetation types.

China's vast expanse spans multiple climatic zones and hosts a diverse array of vegetation types⁵⁰, positioning it as an unrivaled focal point for vegetation phenology research. This study concentrates on the region north of 30°N in China, recognized for its heightened sensitivity to global climate change and suitability for investigating climate impacts on vegetation phenology⁵¹. The NDVI seasonal patterns in this region exhibit pronounced shifts, facilitating the identification of critical climatic periods affecting vegetation. Moreover, satellite-derived vegetation indices in this area are less influenced by solar zenith angles, ensuring enhanced accuracy in extracted vegetation phenology periods relative to southern regions⁵². Agriculture in this northern region predominantly follows one-season and two-season rotations due to simpler cultivation practices³². Thus, our study sheds light on the characteristics of mono- and bi-seasonal vegetation phenology and their responses to climate variables within China's northern region, beyond 30°N.

This study centers on China's middle and high latitudes, employing multi-source data encompassing GIMMS NDVI, relative humidity (RH), shortwave radiation (SR), maximum temperature (Tmax), and minimum temperature (Tmin) spanning from 1982 to 2014. Our aim is to elucidate the relationship between phenology and climate from a comprehensive, macroscopic perspective. Notably, we examine the phenology of two-seasonal vegetation, a facet often overlooked in prior research on vegetation phenology-climate relationships. Over the 1982–2014 timeframe, we hypothesized that easily ignored climate factors may have an effect on vegetation phenology. We analyze how the combined responses of Start of Season (SOS) and End of Season (EOS) relate to pre-season hydrothermal conditions. Furthermore, we explore the interplay between phenology and climatic factors across diverse vegetation types, including Deciduous Needle Leaf Forest (DNF), Deciduous Broadleaf Forest (DBF), Mixed Forest (MF), Grassland (GL), Savanna (SA), and Cropland (CL). This research holds paramount significance in identifying the determinants of vegetation phenology, comprehending the mechanisms steering phenological shifts, and gauging the repercussions of climate change on terrestrial ecosystems.

Methods

Study area

The study area encompasses the temperate region of China situated north of the 30°N latitude, as illustrated in Fig. 1a. To mitigate the influence of changes in non-vegetated land use categories, this study relies on data obtained from the Land Cover Climate Modeling Grid product (MCD12C1) from MODIS satellites, which specifically excludes grids indicating land use changes between 2001 and 2014. Regions characterized as non-vegetated land, including barren land, water bodies, urban and built-up areas, permanent snow and ice, as well as permanent wetlands, were excluded from our analysis. Additionally, vegetation types consisting of fewer than 100 image elements were also excluded. The spatial distribution of vegetation types within the study area is shown in Fig. 1b.

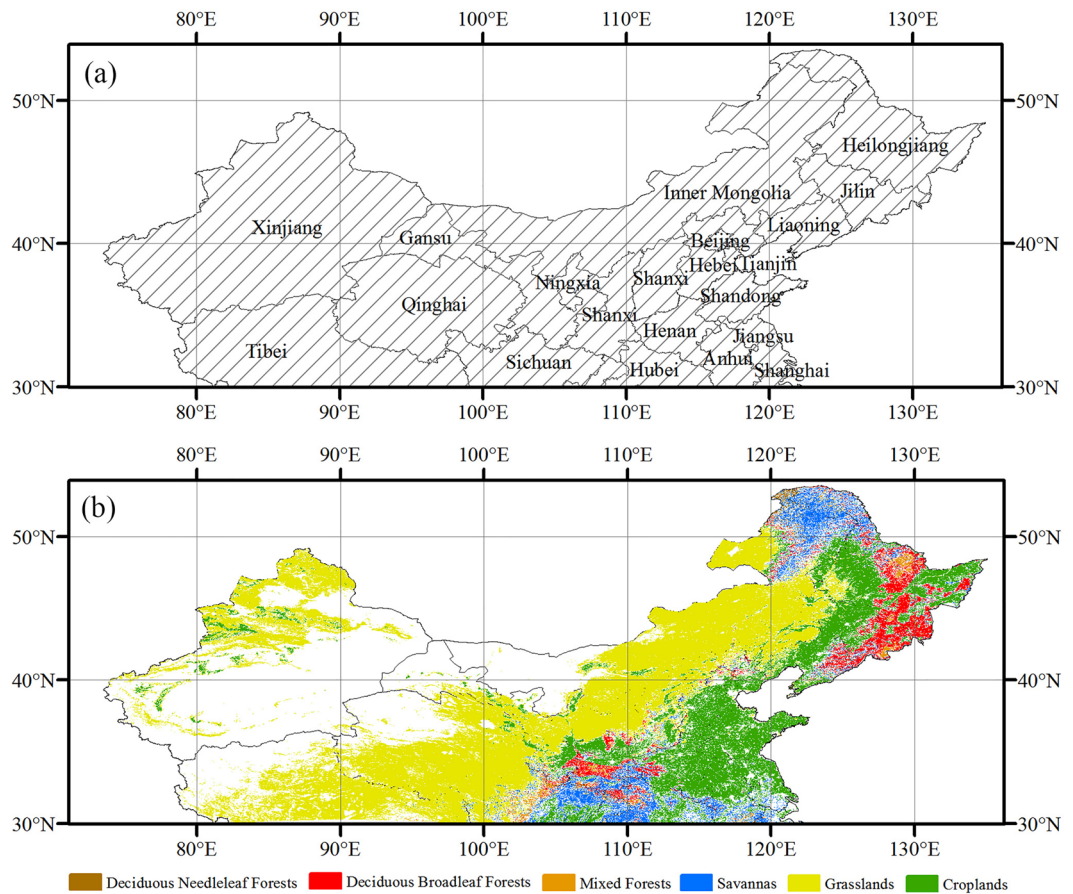


Figure 1. The northern part of China located above the latitude of 30°N (a). Spatial patterns of different vegetation types (b). The basemap was generated by cartopy package (version 0.21.1) in Python 3.9.12 (<https://scitools.org.uk/cartopy/docs/latest/index.html>).

Datasets and preprocessing

We used the National Oceanic and Atmospheric Administration (NOAA) Global Inventory Monitoring and Modeling System (GIMMS) NDVI product, characterized by a spatial resolution of 0.0833333° , to compute key phenology parameters of vegetation spanning from 1982 to 2014. These data products, subject to rigorous quality control measures, have the advantage of offering long time series data and have gained widespread utilization within the field of vegetation phenology research^{53–55}. The extracted vegetation phenology metrics, namely Start of Season (SOS) and End of Season (EOS), underwent validation for accuracy against ground phenology datasets³².

We selected easily neglected climate factors to explore their relationship with vegetation phenology. In particular, in the context of global diurnal asymmetric warming, Tmax and Tmin show different trends⁵⁶, and despite the fact that there is a link between Tmax and Tmin in most cases, their effects on vegetation phenology have been found to be different^{29–31,57}. To align the phenology parameters with the study area, raster data with a spatial resolution of 0.83333° were generated from maximum and minimum temperature, relative humidity, and downward shortwave radiation data. These meteorological data were sourced from 786 monitoring stations spanning the years 1982 to 2014 and were obtained through the China Meteorological Data Network (CMDN) (<http://data.cma.cn/>), employing spline interpolation techniques⁵⁸.

The Land cover data were derived from the Land Cover Climate Modeling Grid product (MCD12C1) from MODIS satellites in 2001 and 2014. These data were resampled to a spatial resolution of 0.83333° using the nearest neighbor method. And non-vegetation land types and vegetation types with fewer than 100 pixels were excluded from the data to obtain the vegetation classification data we need.

Calculation of phenological parameters

The NDVI time series for each pixel was reconstructed using the Savitzky-Golay (SG) filter, preserving pixels with unimodal and bimodal structures (pixels with bimodal structures are candidates for two-season vegetation). The reconstructed NDVI curve is then differentiated to compute the second derivative, enabling the determination of SOS and EOS⁵⁹. Simultaneously, based on ground phenological data, limited time windows for SOS and EOS are defined to accurately extract phenological parameters for different vegetation types. If the SOS and EOS of a particular pixel align with the time window of a single vegetation phenology, it is associated with that vegetation

type. If the SOS and EOS of both growing seasons coincide with the time window of two-season vegetation from ground observations, it is classified as two-season vegetation³².

Statistical analysis

The Pearson correlation analysis was conducted to explore the relationships between SOS and EOS and various climate factors at the pixel level, considering different pre-season lengths. The pre-season climate factor was defined as the average climate factor for the N days leading up to the phenology period within the growing season. In some studies, N is referred to as the "duration of the time window", representing the length of the pre-season, and it typically ranges from 1 to 180⁶⁰.

As shown in Fig. 2, we selected the pre-season length that exhibited the highest absolute Pearson's correlation coefficient as the optimal pre-season length for both vegetation phenology and each pre-season climate factors.

Results

Optimal pre-season length characterization

The spatial pattern of the optimal pre-season length between SOS, EOS and pre-season Tmax is shown in Figs. 3 and 4. The pre-season length in which Tmax presents the greatest impact on SOS is concentrated in the 0–60 days. The optimal pre-season length in northern Inner Mongolia and northern Heilongjiang is dominated by 20–40 days. In contrast, the optimal pre-season length in the intersection between the Liaoning, the Jilin, and the Inner Mongolia provinces is dominated by 120–180 days. The pre-season length where the pre-season Tmax exhibits the largest impact on EOS is centered on the 0–20 days and 160–180 days. The optimal pre-season length is 140–180 days in large areas of northern Heilongjiang and northern Inner Mongolia.

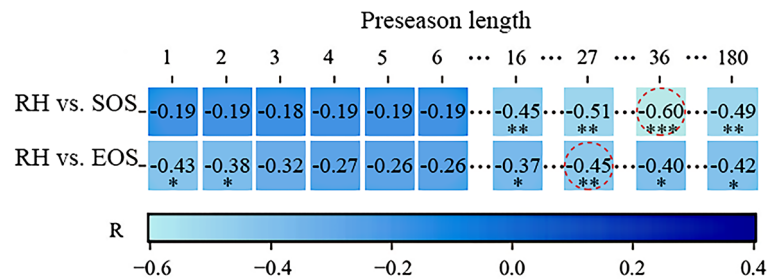


Figure 2. The matrix of correlation coefficients. The red dashed circle indicates the highest value within each row, with its associated pre-season length representing the optimal length (significance levels are indicated by *** for $p < 0.001$, ** for $p < 0.01$, and * for $p < 0.05$).

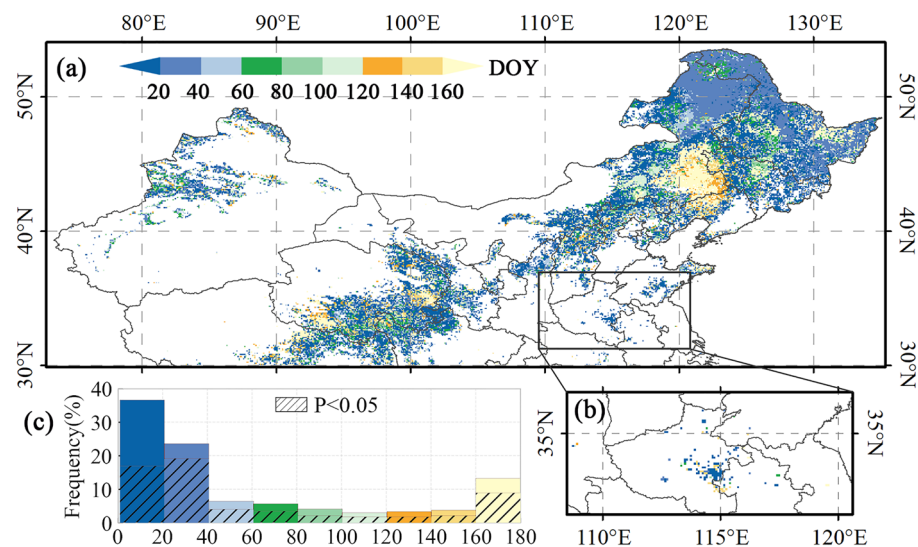


Figure 3. Spatial patterns of SOS and pre-season Tmax optimal pre-season length in (a) single-season vegetation, first season of two-season vegetation, and (b) second season of two-season vegetation. (c) Histograms of the optimal pre-season length. The basemap was generated by cartopy package (version 0.21.1) in Python 3.9.12 (<https://scitools.org.uk/cartopy/docs/latest/index.html>).

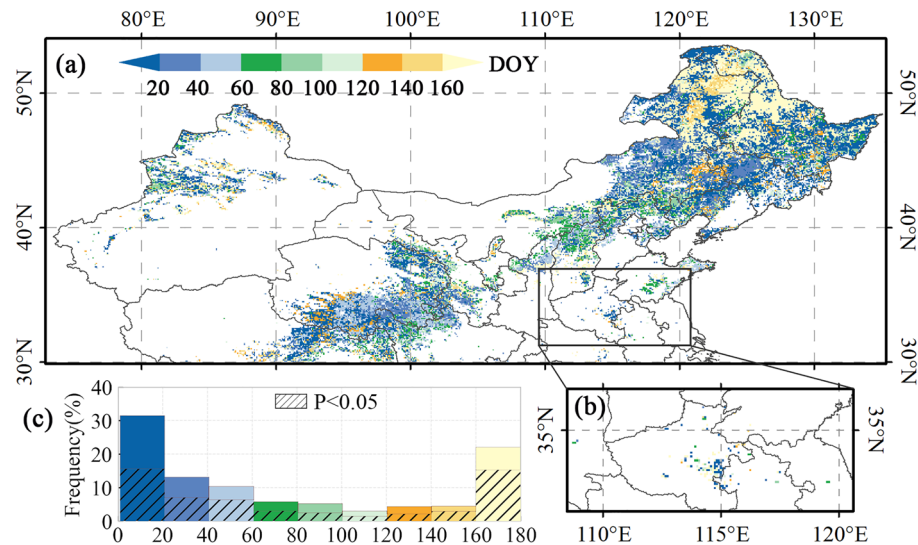


Figure 4. Spatial patterns of EOS and preseason Tmax optimal preseason length in (a) single-season vegetation, first season of two-season vegetation, and (b) second season of two-season vegetation. (c) Histograms of the optimal preseason length. The basemap was generated by cartopy package (version 0.21.1) in Python 3.9.12 (<https://scitools.org.uk/cartopy/docs/latest/index.html>).

Characterization of vegetation phenology in response to climatic factors

The spatial distribution of vegetation SOS and preseason Tmax correlations, trend slopes, and significance are shown in Fig. 5. Vegetation SOS is significantly correlated with the preseason Tmax in 60.4% of the region of interest. Among them, about 16.25% of the areas show a significant positive correlation, and 44.15% have a significant negative correlation. Significant negative correlation dominates in northern Inner Mongolia, Heilongjiang and Jilin provinces. The SOS is generally significantly positively correlated with the preseason Tmax in areas such as the junction of Inner Mongolia and Liaoning. Significant negative correlations between SOS and preseason Tmax dominate in both the first and second seasons of the two-season vegetation.

The spatial distribution of vegetation SOS and preseason Tmin correlations, trend slopes, and significance are shown in Fig. 6. The vegetation SOS is significantly correlated with preseason Tmin in 57.59% of the areas in the study area. Among them, about 15.34% of the areas show a significant positive correlation, and 42.25% have a significant negative correlation. Significant negative correlation dominates in northern Inner Mongolia, Heilongjiang and Jilin provinces. The SOS is generally significantly positively correlated with the preseason Tmin in areas such as the junction of Inner Mongolia and Liaoning. Negative correlations between SOS and preseason Tmin were dominant in both the first and second seasons of the two-season vegetation.

The spatial distribution of vegetation EOS and preseason SR correlations, trend slopes, and significance is shown in Fig. 7. The vegetation EOS is significantly correlated with preseason SR in 61.32% of the studied regions. Among these, about 12.29% (49.03%) exhibit a significant positive (negative) correlation. The intersection between Inner Mongolia and Heilongjiang Province and other places is dominated by a significant negative correlation. Areas such as the intersection between Inner Mongolia and Liaoning and the southern part of the Qinghai Province generally present a significant positive correlation between EOS and preseason SR. Significant positive correlations are found between EOS and preseason SR in both the first and second seasons of the two-season vegetation.

Response characteristics of different vegetation phenology to climatic factors

Figure 8 shows the distribution of regions with different R-values of SOS and preseason RH for different types of vegetation. In DNF, DBF and SA, SOS and preseason RH mainly show a significant positive correlation, accounting for 62.58%, 74.52% and 83.36%, respectively. In MF and CL, SOS and preseason RH generally show a significant positive correlation, accounting for 51.84% and 44.13%, respectively, and some areas show a significant negative correlation, accounting for 4.41% and 14.68%, respectively. In GL, SOS is significantly positively correlated with pre-season RH in 21.12% of the areas and significantly negatively correlated with preseason RH in 24.96%.

Figure 9 shows the frequency distribution of regions with different R-values of EOS and preseason RH for different types of vegetation. In DNF, DBF, MF and SA, EOS shows a generally significant positive correlation with preseason RH, with percentages of 46.45%, 42.18%, 43.00% and 70.64%, respectively. In GL, 21.34% of the area shows a significant positive correlation between EOS and preseason RH, and 21.58% is significantly negative correlation between EOS and preseason RH. In CL, 10.87% of area EOS is significantly positively correlated with preseason RH, and 35.35% of area EOS is significantly negatively correlated with preseason RH.

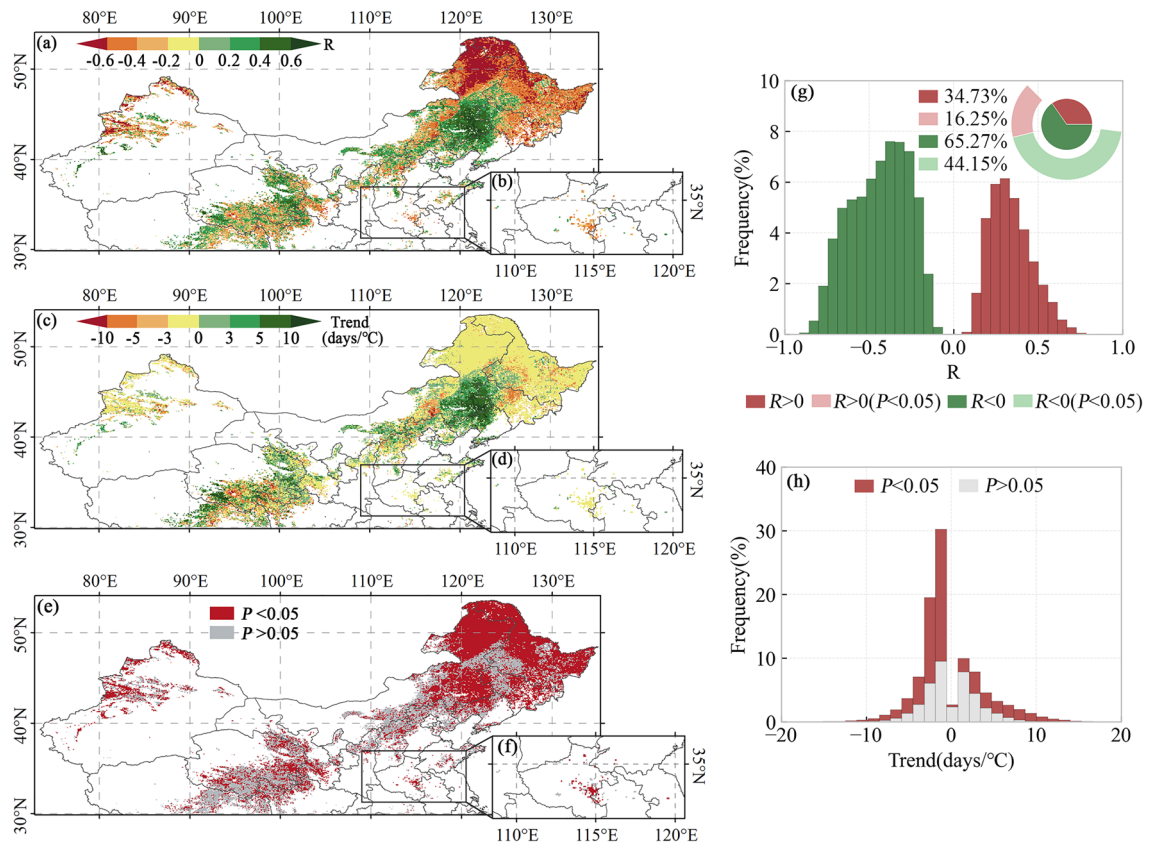


Figure 5. Spatial patterns of R-values (a, b), slopes (c, d), and P-values (e, f) of SOS vs. pre-season Tmax for single-season vegetation (a, c, e), first season of two-season vegetation (a, c, d), and second season of two-season vegetation (b, d, f). Histograms of frequency distributions of R-values (g) and trends (h). The basemap was generated by cartopy package (version 0.21.1) in Python 3.9.12 (<https://scitools.org.uk/cartopy/docs/latest/index.html>).

Figure 10 shows the distribution of regions with different R-values of SOS and pre-season Tmax for different types of vegetation. In DNF, DBF and savanna, SOS and pre-season Tmax are significantly negatively correlated with each other, accounting for 99.35%, 84.36% and 96.04%, respectively. In MF and CL, SOS and pre-season Tmax are significantly negatively correlated, with a larger percentage of 46.32% and 48.18%, respectively. In GL, EOS and pre-season Tmax are significantly positively correlated in 22.88% of the area, and significantly negatively correlated in 26.5%.

Figure 11 shows the distribution of regions with different R-values of EOS and pre-season Tmax for different types of vegetation. In DNF, SA and MF, EOS and pre-season Tmax are significantly positively correlated, accounting for 96.13%, 84.95% and 50.37%, respectively. In DBF, EOS and pre-season Tmax are significantly positively correlated in 26.25% of the areas and significantly negatively correlated in 15.76%. In GL, 36.8% of the area has a significant positive correlation between EOS and pre-season Tmax, and 17.9% of the area has a significant negative correlation. In CL, 23.78% of the areas have a significant positive correlation between EOS and pre-season Tmax and 22.9% of the areas have significant negative correlation.

Figure 12 shows the distribution of regions with different R-values of SOS and pre-season Tmin for different types of vegetation. In DNF, DBF, SA, SOS and pre-season Tmin are significantly negatively correlated with each other, accounting for 98.71%, 76.57% and 93.48%, respectively. In MF and CL, SOS and pre-season Tmin are significantly negatively correlated with a larger percentage of 45.59% and 46.05%, respectively. In GL, SOS and pre-season Tmin are significantly positively correlated in 20.85% of the areas and significantly negatively correlated in 25.05%.

Discussion

When comparing RH and optimal pre-season length of vegetation SOS (Fig. S1), we observe a rapid response of vegetation to changes in humidity. This response was particularly evident in regions such as northern Inner Mongolia and northern Heilongjiang, where the optimal pre-season length consistently ranged from 20 to 40 days. Remarkably, this contrasted with the situation at the intersection of Liaoning, Jilin, and Inner Mongolia provinces, where the optimal pre-season length was prolonged, ranging from 120 to 180 days. Similar results were observed when studying the effect of RH on EOS (Fig. S2). These differences may be attributed to the complex interactions of regional climate change. When considering the effects of SR, different trends emerge (Fig. S3). A

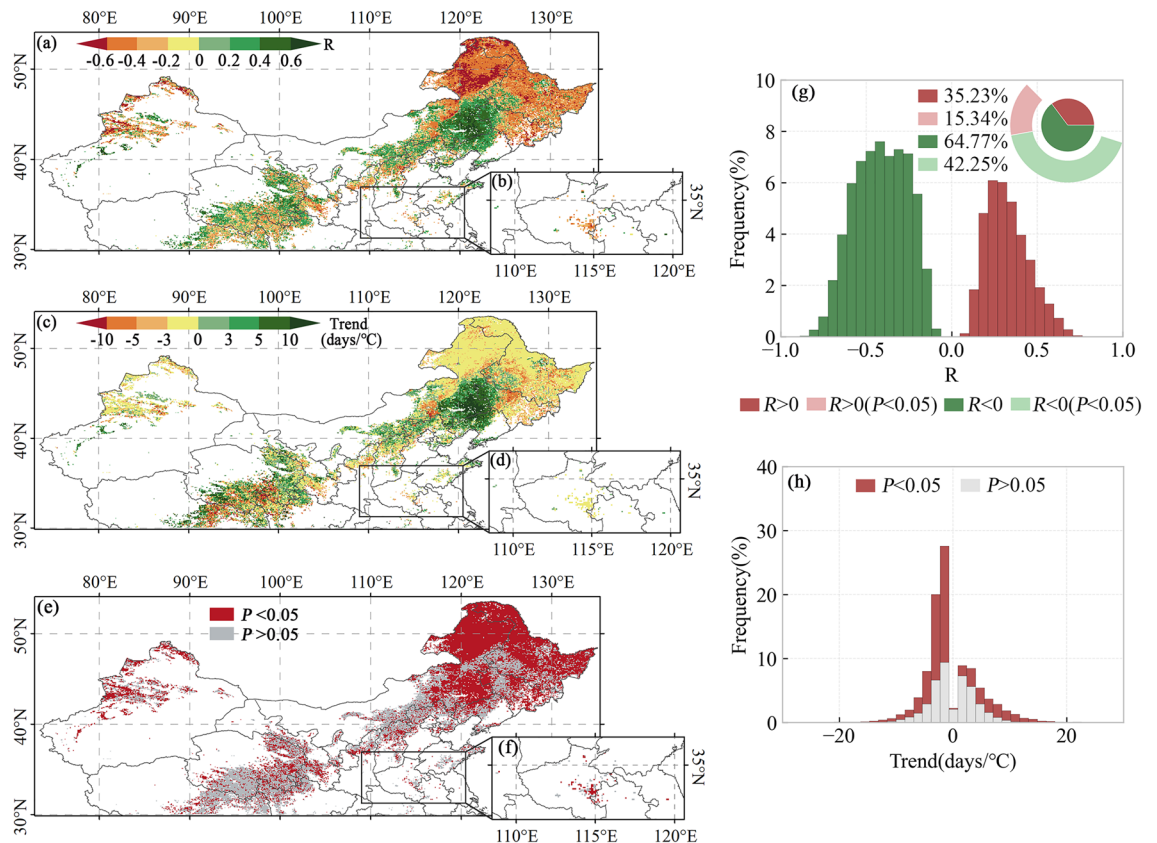


Figure 6. Spatial patterns of R-values (a, b), slopes (c, d), and P-values (e, f) of SOS vs. pre-season T_{min} for single-season vegetation (a, c, e), first season of two-season vegetation (a, c, d), and second season of two-season vegetation (b, d, f). Histograms of frequency distributions of R-values (g) and trends (h). The basemap was generated by cartopy package (version 0.21.1) in Python 3.9.12 (<https://scitools.org.uk/cartopy/docs/latest/index.html>).

preseason length of 0–20 days is critical for SOS effects, while a broader preseason length of 0–60 days affects EOS (Fig. S4). This difference may be attributed to differences in the sensitivity of SOS and EOS to SR. Additionally, the optimal preseason length for both SOS and EOS predominantly falls within 120–180 days, during the first and second seasons of the two-season vegetation. Biseasonal vegetation needs a longer period for photosynthesis and growth. It has been noted that SR predominates in the phenology of biseasonal vegetation⁶¹. This suggests that prolonged exposure to short-wave radiation is critical for the growth phase of the two-season vegetation. Solar radiation plays a key role in the photosynthesis and vegetation activity during the growing season²⁷, for instance, its influence on plant growth response along with pre-season radiation intensity constitutes a significant factor affecting the spatial differentiation of phenology in temperate deciduous forests⁶². The preseason length in which both T_{max} and T_{min} have the greatest effect on SOS is primarily centered on days 0 to 60 (Fig. S5).

The onset of vegetation growth requires sufficient heat accumulation⁶³. Generally, the temperature of the region needs to reach 0–5 °C to break the vegetation dormancy and start growth⁶⁴. Therefore, increased temperature accelerates heat accumulation, promoting vegetation germination. The preseason of 0–60 days corresponds to the dormant period of vegetation, which is the main reason why the optimal preseason length for SOS and temperature is concentrated within this range. However, there are regions where the optimal preseason length for EOS and temperature is concentrated at 120–180 days. This may be due to the fact that the heat required for vegetation growth can accumulate rapidly due to warmer spring temperatures, leading to rapid vegetation growth. The climate effect on spring phenology further carries over to fall phenology through carryover effects^{63,65}.

The relationship between vegetation SOS and EOS and preseason RH (Figs. S7, S8), SR, and temperature showed different trends across growing seasons and regions. RH influences seed germination and seedling growth in plants. Higher RH can facilitate rapid seed water absorption and germination under appropriate moisture conditions, favoring earlier crop growth². However, excessive moisture may lead to overly wet soil, affecting seed oxygen supply root system growth, thereby delaying the onset of growth.

In some areas, we observed a significant positive correlation between preseason SR and SOS (Fig. S9), where an increase in SR may lead to a delay in the start date of vegetation growth. This could be attributed to increased SR resulting in higher surface temperatures, which may inhibit seed germination or seedling growth. Conversely, in other regions, we observed a significant negative correlation between preseason SR and SOS. Higher SR provides more energy to induce photosynthesis and plant growth. In most areas, there was a significant negative correlation between preseason SR and EOS (Fig. 7)^{1,57}, indicating that an increase in SR accelerates EOS. This may be

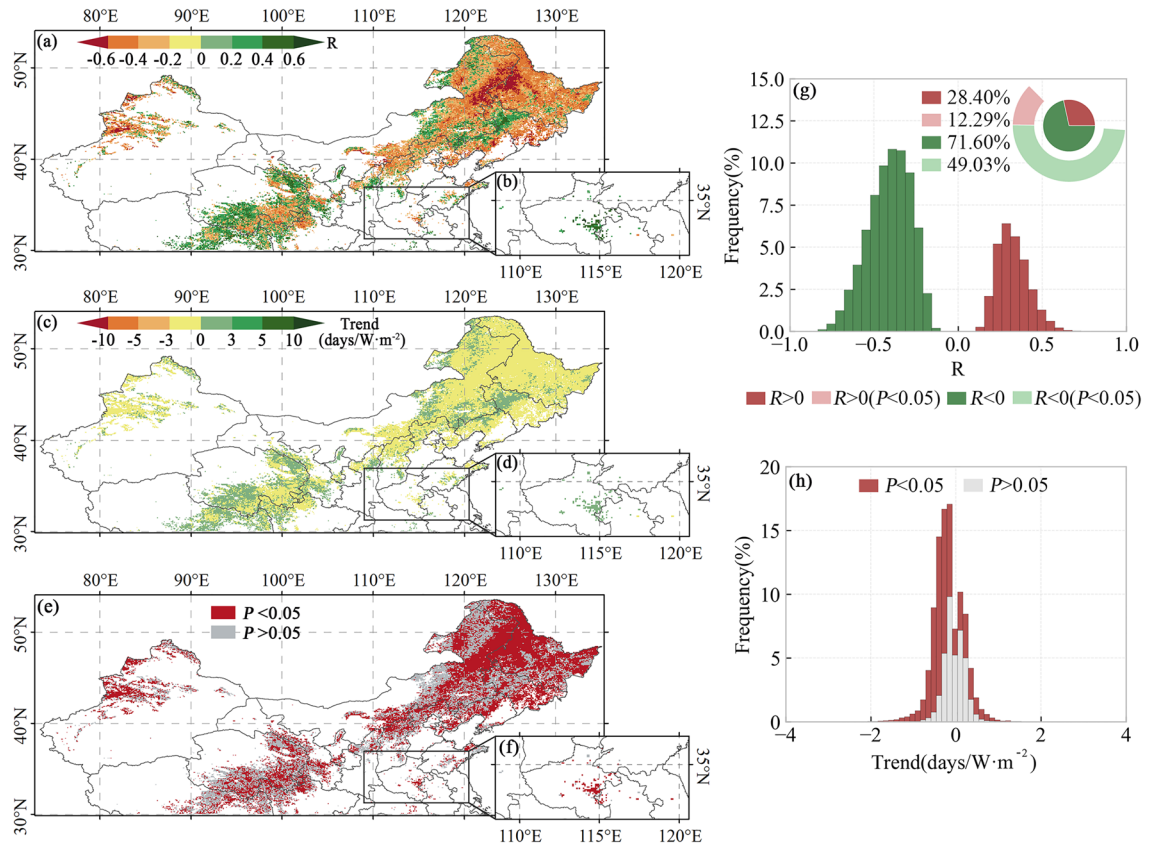


Figure 7. Spatial patterns of R-values (a, b), slopes (c, d), and P-values (e, f) of EOS vs. preseason SR for single-season vegetation (a, c, e), first season of two-season vegetation (a, c, d), and second season of two-season vegetation (b, d, f). Histograms of frequency distributions of R-values (g) and trends (h). The basemap was generated by cartopy package (version 0.21.1) in Python 3.9.12 (<https://scitools.org.uk/cartopy/docs/latest/index.html>).

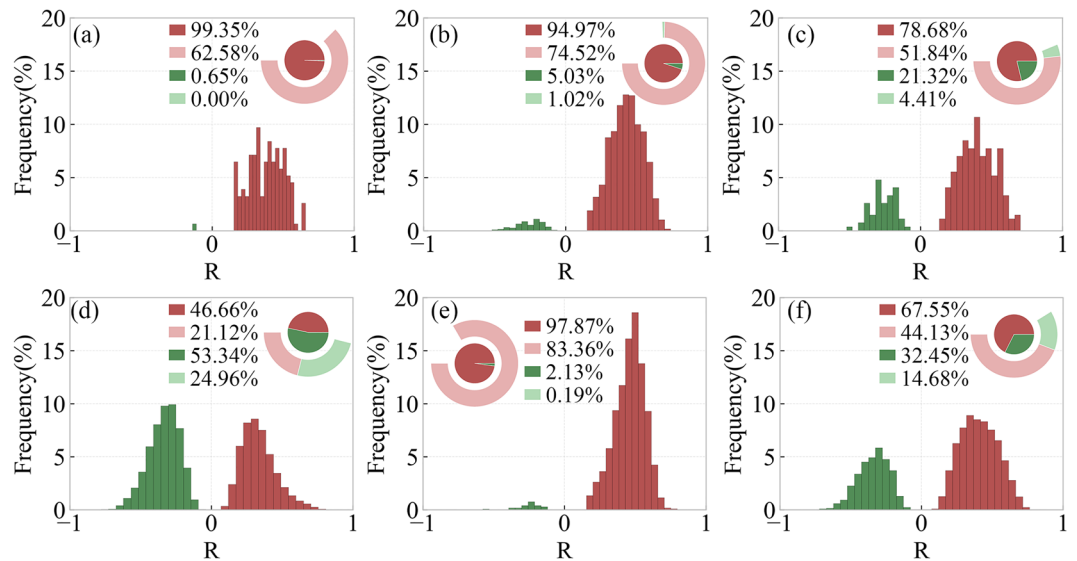


Figure 8. Frequency distribution of regions with different R-values of SOS and preseason RH for different types of vegetation including DNF (a), DBF (b), MF (c), GL (d), SA (e), CL (f).

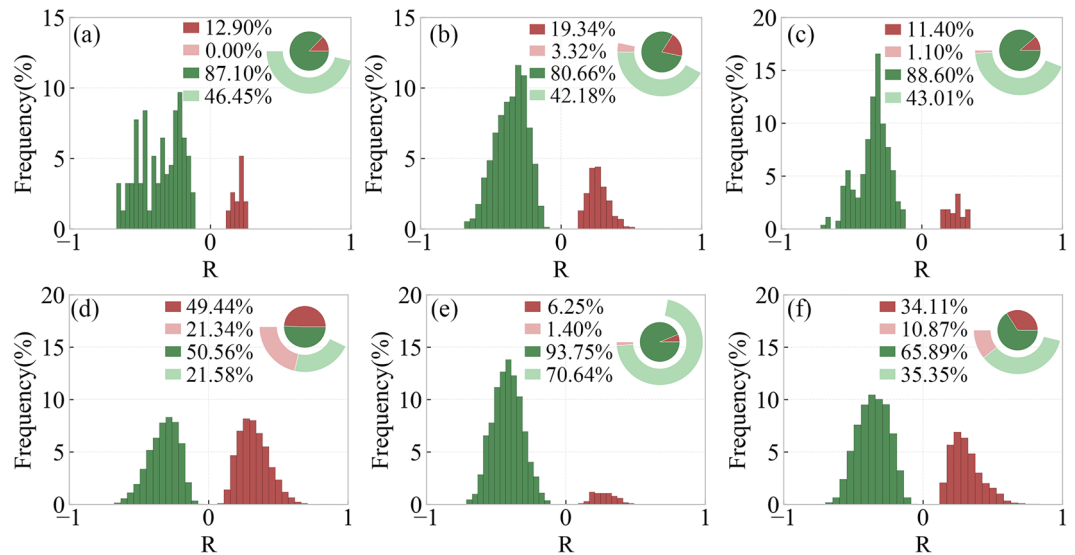


Figure 9. Frequency distribution of regions with different R-values of EOS and pre-season RH for different types of vegetation including DNF (a), DBF (b), MF (c), GL (d), SA (e), CL (f).

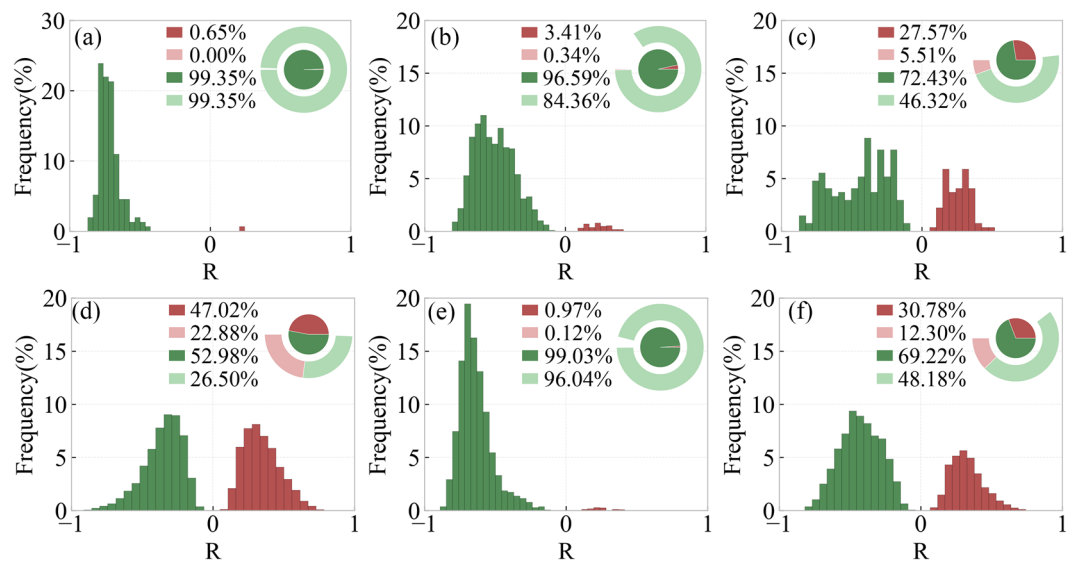


Figure 10. Frequency distribution of regions with different R-values of SOS and pre-season Tmax for different types of vegetation including DNF (a), DBF (b), MF (c), GL (d), SA (e), CL (f).

attributed to the fact that plants complete their life cycle more rapidly under increased light conditions¹⁹. When leaf absorption of light energy exceeds its photosynthetic capacity, it leads to an increase in plant leaf xanthophylls and anthocyanins, promoting leaf aging⁶⁶. Simultaneously, the enhanced photosynthesis resulting from increased solar radiation accelerates carbon saturation and speeds up the aging process^{67,68}. Additionally, pre-season Tmax and Tmin were both significantly negatively correlated with vegetation SOS and significantly positively correlated with vegetation EOS in most areas (Figs. S10, S11)^{1,19}. This implies that warmer temperatures in most areas will accelerate vegetation SOS and delay vegetation EOS³. Sufficient heat accumulation is required for the onset of vegetation growth, and warmer temperatures expedite this process, promoting vegetation germination^{60,69}. Higher temperatures in summer and fall have been reported to enhance the activity of photosynthetic enzymes and reduce the rate of chlorophyll degradation, leading to a delay in EOS^{54,70,71}. Furthermore, nighttime warming may contribute to the positive effects of pre-season temperatures on EOS by reducing the risk of freezing due to low temperatures and slowing the leaf coloration process⁷².

This study reveals the diversity and complexity of vegetation responses to climate change by analyzing the relationship between phenology and easily ignored climatic factors in various vegetation types. Both SOS and EOS were significantly positively correlated with RH in SA north of 30°N in China, indicating that RH was the dominant climatic factor for SA phenology. Significant negative correlations between SOS and Tmax and Tmin

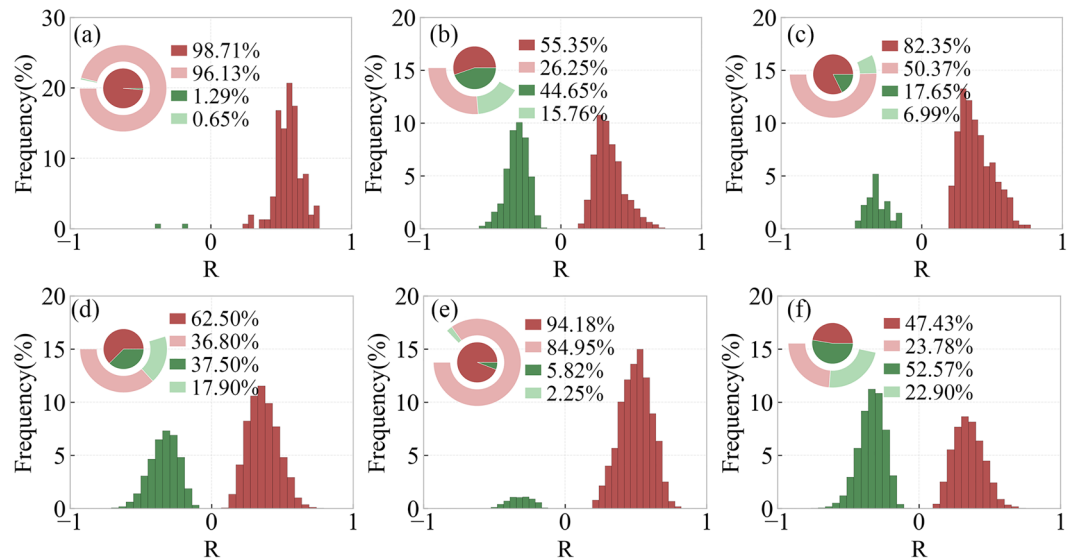


Figure 11. Frequency distribution of regions with different R-values of EOS and preseason Tmax for different types of vegetation including DNF (a), DBF (b), MF (c), GL (d), SA (e), CL (f).

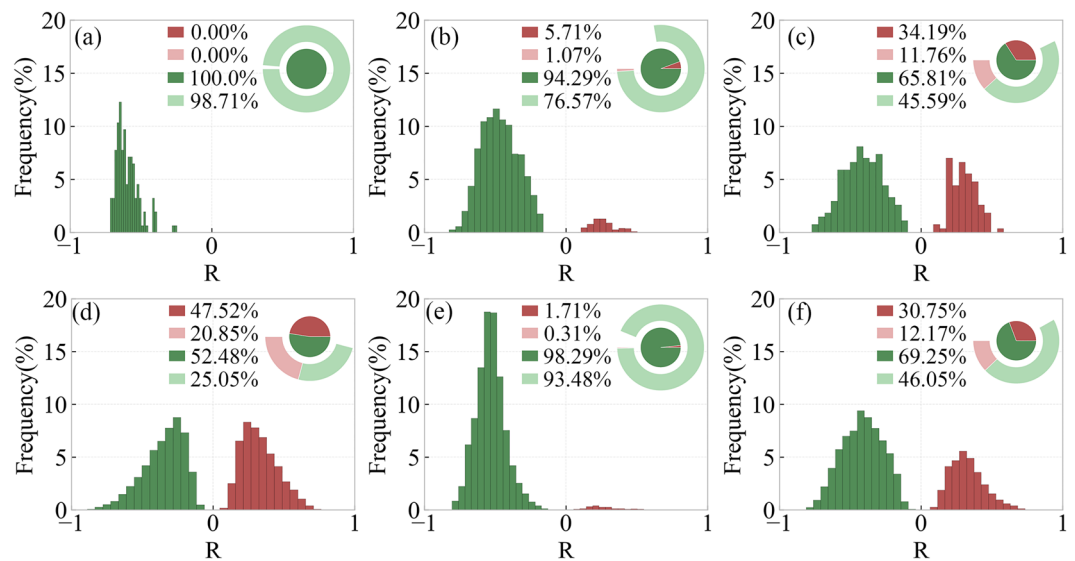


Figure 12. Frequency distribution of regions with different R-values of SOS and preseason Tmin for different types of vegetation including DNF (a), DBF (b), MF (c), GL (d), SA (e), CL (f).

in DNF, DBF, and GL, suggesting that temperature strongly influences SOS in these three vegetation types. Additionally, the significant positive correlation between EOS and Tmax in DNF indicates that EOS in DNF is predominantly influenced by Tmin. How different vegetation types react to climatic factors is diverse, involving factors such as vegetation growth characteristics, ecological adaptations, and physiological mechanisms²⁹. In various vegetation types, the link between phenology and climatic factors may be jointly influenced by several factors, such as growth strategy, photosynthetic efficiency, and water use efficiency^{6,8,73}. The same vegetation type exhibited different patterns of relationships under different climate factors, suggesting a diversity of strategies for vegetation to adapt to climate change.

Conclusion

In this research, we focused on the mid-to-high latitude region of China as our study area and we leveraged the GIMMS NDVI 3g long time series remote sensing dataset to extract climate parameters for different vegetation types at the raster level. Our analysis spanned the years 1982 to 2014, and our primary goal was to investigate the interplay between vegetation phenology and easily ignored climate elements. To accomplish this, we constructed correlation coefficient matrices between preseason RH, SR, Tmax, Tmin and vegetation phenology (SOS/EOS)

at various raster locations. This allowed us to explore how different climate factors influence various vegetation phenology parameters within their optimal pre-season length. The key findings of this study are as follows:

- (1) We observed that the optimal pre-season lengths for RH, SR, Tmax, and Tmin, which exert the most significant influence on vegetation phenology, exhibited variability across different regions and growing seasons of vegetation. In most regions, the optimal pre-season length influencing vegetation phenology fell within the range of 0–60 days.
- (2) Our analysis revealed diverse trends in the relationships between SOS, EOS, and pre-season RH, SR, and temperature across different growing seasons and regions. Specifically, pre-season RH exhibited a significant positive correlation with vegetation SOS in 37.86% of the areas, while it showed a significant negative correlation with vegetation EOS in 32.73% of the areas. Pre-season SR was significantly negatively correlated with vegetation EOS in 49.03% of the areas. Furthermore, both pre-season Tmax and Tmin displayed significant negative correlations with vegetation SOS in 44.15% and 42.25% of the areas, respectively.
- (3) The interactions between phenology and climate factors in various vegetation types were characterized by their diversity and complexity. Within the northern region of China, RH emerged as the dominant climatic factor influencing the phenology of SA vegetation. Temperature, on the other hand, exerted strong control over the SOS in three distinct vegetation types, namely DNE, DBF, and SA. Additionally, the EOS of DNF vegetation was predominantly governed by Tmax.

Overall, our research sheds light on the intricate relationships between climate and vegetation phenology, providing valuable insights into the dynamics of ecosystems in the mid-to-high latitude region of China.

Data availability

The datasets analyzed during the current study available from the corresponding author on reasonable request.

Code availability

The source codes for the analysis of this study are available from the corresponding author upon reasonable request.

Received: 27 January 2024; Accepted: 9 April 2024

Published online: 16 April 2024

References

1. Peng, J., Wu, C., Wang, X. & Lu, L. Spring phenology outweighed climate change in determining autumn phenology on the Tibetan Plateau. *Int. J. Climatol.* **41**, 3725–3742. <https://doi.org/10.1002/joc.7045> (2021).
2. Ren, S. & An, S. Temporal pattern analysis of cropland phenology in Shandong province of China based on two long-sequence remote sensing data. *Remote Sensing* **13**, 4071. <https://doi.org/10.3390/rs13204071> (2021).
3. Li, Z. *et al.* Assessment of climatic impact on vegetation spring phenology in Northern China. *Atmosphere* **14**, 117. <https://doi.org/10.3390/atmos14010117> (2023).
4. Fan, J., Min, J., Yang, Q., Na, J. & Wang, X. Spatial-temporal relationship analysis of vegetation phenology and meteorological parameters in an agro-pasture ecotone in China. *Remote Sensing* **14**, 5417. <https://doi.org/10.3390/rs14215417> (2022).
5. Chen, H., Wang, Q., Bento, V. A., Meng, X. & Li, X. Vegetation drought risk assessment based on the multi-weight methods in Northwest China. *Environ. Monitor. Assessm.* **195**, 1148. <https://doi.org/10.1007/s10661-023-11747-z> (2023).
6. Cui, X., Xu, G., He, X. & Luo, D. Influences of seasonal soil moisture and temperature on vegetation phenology in the Qilian mountains. *Remote Sensing* **14**, 3645. <https://doi.org/10.3390/rs14153645> (2022).
7. Li, H., Feng, J., Bai, L. & Zhang, J. Populus euphratica phenology and its response to climate change in the upper Tarim River Basin NW China. *Forests* **12**, 1315. <https://doi.org/10.3390/f12101315> (2021).
8. Wang, C. *et al.* Comparison of vegetation phenology derived from solar-induced chlorophyll fluorescence and enhanced vegetation index, and their relationship with climatic limitations. *Remote Sensing* **14**, 3018. <https://doi.org/10.3390/rs14133018> (2022).
9. Wan, L. *et al.* Drought characteristics and dominant factors across China: Insights from high-resolution daily SPEI dataset between 1979 and 2018. *Sci. Total Environ.* **901**, 166362. <https://doi.org/10.1016/j.scitotenv.2023.166362> (2023).
10. Zhang, R. *et al.* The first high spatial resolution multi-scale daily SPI and SPEI raster dataset for drought monitoring and evaluating over China from 1979 to 2018. *Big Earth Data* **7**, 860–885. <https://doi.org/10.1080/20964471.2022.2148331> (2023).
11. Lei, L. *et al.* Plant feedback aggravates soil organic carbon loss associated with wind erosion in northwest China. *J. Geophys. Res. Biogeosci.* **124**, 825–839. <https://doi.org/10.1029/2018JG004804> (2019).
12. Wang, Q. *et al.* Freeze-Thaw cycle representation alters response of watershed hydrology to future climate change. *Catena* **195**, 104767. <https://doi.org/10.1016/j.catena.2020.104767> (2020).
13. Zeng, J. *et al.* Improving the drought monitoring capability of VHI at the global scale via ensemble indices for various vegetation types from 2001 to 2018. *Weather Clim. Extrem.* **35**, 100412. <https://doi.org/10.1016/j.wace.2022.100412> (2022).
14. Wang, Q. F. *et al.* A multi-scale daily SPEI dataset for drought characterization at observation stations over mainland China from 1961 to 2018. *Earth Syst. Sci. Data* **13**, 331–341. <https://doi.org/10.5194/essd-13-331-2021> (2021).
15. Xu, F. *et al.* Understanding climate change impacts on drought in China over the 21st century: A multi-model assessment from CMIP6. *NPJ Clim. Atmosph. Sci.* **7**, 32. <https://doi.org/10.1038/s41612-024-00578-5> (2024).
16. Zhang, J., Chen, S. Z., Wu, Z. F. & Fu, Y. H. Review of vegetation phenology trends in China in a changing climate. *Progress Phys. Geograph. Earth Environ.* **46**, 829–845. <https://doi.org/10.1177/03091333221114737> (2022).
17. Tao, Z., Wang, H., Liu, Y., Xu, Y. & Dai, J. Phenological response of different vegetation types to temperature and precipitation variations in northern China during 1982–2012. *Int. J. Remote Sensing* **38**, 3236–3252. <https://doi.org/10.1080/01431161.2017.1292070> (2017).
18. Bonan, G. B. Forests and climate change: Forcings, feedbacks, and the climate benefits of forests. *Science* **320**, 1444–1449. <https://doi.org/10.1126/science.1155121> (2008).
19. Gao, X. & Zhao, D. Impacts of climate change on vegetation phenology over the Great Lakes Region of Central Asia from 1982 to 2014. *Sci. Total Environ.* **845**, 157227. <https://doi.org/10.1016/j.scitotenv.2022.157227> (2022).
20. Wu, X. *et al.* The effect of drought on vegetation gross primary productivity under different vegetation types across China from 2001 to 2020. *Remote Sensing* <https://doi.org/10.3390/rs14184658> (2022).

21. Wang, T. *et al.* Hysteretic effects of meteorological conditions and their interactions on particulate matter in Chinese cities. *J. Clean. Product.* **274**, 122926. <https://doi.org/10.1016/j.jclepro.2020.122926> (2020).
22. Li, Z. *et al.* Responses of vegetation autumn phenology to climatic factors in northern China. *Sustainability* **14**, 8590. <https://doi.org/10.3390/su14148590> (2022).
23. Marchin, R. M., Salk, C. F., Hoffmann, W. A. & Dunn, R. R. Temperature alone does not explain phenological variation of diverse temperate plants under experimental warming. *Glob. Change Biol.* **21**, 3138–3151. <https://doi.org/10.1111/gcb.12919> (2015).
24. Peng, Q., Wang, R., Jiang, Y. & Li, C. Contributions of climate change and human activities to vegetation dynamics in Qilian Mountain National Park, Northwest China. *Glob. Ecol. Conserv.* **32**, e01947. <https://doi.org/10.1016/j.gecco.2021.e01947> (2021).
25. de Azevedo, I. F. P. *et al.* Phenology of riparian tree species in a transitional region in southeastern Brazil. *Brazil. J. Bot.* **37**, 47–59. <https://doi.org/10.1007/s40415-014-0046-5> (2014).
26. Goulart, M. F., Lemos-Filho, J. P. & Lovato, M. B. Phenological variation within and among populations of *Plathymenia reticulata* in Brazilian Cerrado, the Atlantic forest and transitional sites. *Ann. Bot.* **96**, 445–455. <https://doi.org/10.1093/aob/mci193> (2005).
27. Gui, X. *et al.* Environmental factors modulate the diffuse fertilization effect on gross primary productivity across Chinese ecosystems. *Sci. Total Environ.* **793**, 148443. <https://doi.org/10.1016/j.scitotenv.2021.148443> (2021).
28. Guo, J. *et al.* Specific drivers and responses to land surface phenology of different vegetation types in the Qinling Mountains Central China. *Remote Sensing* **13**, 4538. <https://doi.org/10.3390/rs13224538> (2021).
29. Liu, Y. *et al.* Variation in vegetation phenology and its response to climate change in marshes of inner Mongolian. *Plants* **12**, 2072. <https://doi.org/10.3390/plants12112072> (2023).
30. Wang, J. *et al.* Contrasting temporal variations in responses of leaf unfolding to daytime and night-time warming. *Glob. Change Biol.* **27**, 5084–5093. <https://doi.org/10.1111/gcb.15777> (2021).
31. Wu, C. Y. *et al.* Contrasting responses of autumn-leaf senescence to daytime and night-time warming. *Nat. Clim. Change* **8**, 1092–1096. <https://doi.org/10.1038/s41558-018-0380-x> (2018).
32. Zhang, R., Qi, J., Leng, S. & Wang, Q. Long-term vegetation phenology changes and responses to pre-season temperature and precipitation in Northern China. *Remote Sensing* **14**, 1396. <https://doi.org/10.3390/rs14061396> (2022).
33. Ren, Y. *et al.* Earlier spring greening in Northern Hemisphere terrestrial biomes enhanced net ecosystem productivity in summer. *Commun. Earth Environ.* **5**, 122. <https://doi.org/10.1038/s43247-024-01270-5> (2024).
34. Hasan, M. A. *et al.* Temporal changes in land cover, land surface temperature, soil moisture, and evapotranspiration using remote sensing techniques—A case study of Kutupalong Rohingya Refugee Camp in Bangladesh. *J. Geovis. Spat. Anal.* **7**, 11. <https://doi.org/10.1007/s41651-023-00140-6> (2023).
35. Tabassum, A. *et al.* Exploring the relationship between land use land cover and land surface temperature: A case study in Bangladesh and the policy implications for the global South. *J. Geovis. Spat. Anal.* **7**, 25. <https://doi.org/10.1007/s41651-023-00155-z> (2023).
36. Tang, J. *et al.* Self-adapting extraction of cropland phenological transitions of rotation agroecosystems using dynamically fused NDVI images. *Int. J. Biometeorol.* **64**, 1273–1283. <https://doi.org/10.1007/s00484-020-01904-1> (2020).
37. Piao, S., Mohammat, A., Fang, J., Cai, Q. & Feng, J. NDVI-based increase in growth of temperate grasslands and its responses to climate changes in China. *Glob. Environ. Change* **16**, 340–348. <https://doi.org/10.1016/j.gloenvcha.2006.02.002> (2006).
38. Jonsson, P. & Eklundh, L. TIMESAT: A program for analyzing time-series of satellite sensor data. *Comput. Geosci.* **30**, 833–845. <https://doi.org/10.1016/j.cageo.2004.05.006> (2004).
39. Jönsson, P., Cai, Z., Melaas, E., Friedl, M. & Eklundh, L. A method for robust estimation of vegetation seasonality from landsat and sentinel-2 time series data. *Remote Sensing* **10**, 635. <https://doi.org/10.3390/rs10040635> (2018).
40. Sakamoto, T. *et al.* A crop phenology detection method using time-series MODIS data. *Remote Sensing Environ.* **96**, 366–374. <https://doi.org/10.1016/j.rse.2005.03.008> (2005).
41. Moody, A. & Johnson, D. M. Land-surface phenologies from AVHRR using the discrete Fourier transform. *Remote Sensing Environ.* **75**, 305–323. [https://doi.org/10.1016/S0034-4257\(00\)00175-9](https://doi.org/10.1016/S0034-4257(00)00175-9) (2001).
42. Ibrahim, S. A., Kaduk, J., Tansey, K., Balzter, H. & Lawal, U. M. Detecting phenological changes in plant functional types over West African savannah dominated landscape. *Int. J. Remote Sensing* **42**, 567–594. <https://doi.org/10.1080/01431161.2020.1811914> (2020).
43. Wang, X. F. *et al.* Validation of MODIS-GPP product at 10 flux sites in northern China. *Int. J. Remote Sensing* **34**, 587–599. <https://doi.org/10.1080/01431161.2012.715774> (2013).
44. Feng, S. *et al.* Improved estimation of vegetation water content and its impact on L-band soil moisture retrieval over cropland. *J. Hydrol.* **617**, 129015. <https://doi.org/10.1016/j.jhydrol.2022.129015> (2023).
45. White, M. A., Thornton, P. E. & Running, S. W. A continental phenology model for monitoring vegetation responses to interannual climatic variability. *Glob. Biogeochem. Cycl.* **11**, 217–234. <https://doi.org/10.1029/97gb00330> (1997).
46. Tan, B. *et al.* An enhanced TIMESAT algorithm for estimating vegetation phenology metrics from MODIS data. *IEEE J. Select. Top. Appl. Earth Observ. Remote Sensing* **4**, 361–371. <https://doi.org/10.1109/JSTARS.2010.2075916> (2011).
47. Luo, Y. C., Zhang, Z., Chen, Y., Li, Z. Y. & Tao, F. L. ChinaCropPhen1km: a high-resolution crop phenological dataset for three staple crops in China during 2000–2015 based on leaf area index (LAI) products. *Earth Syst. Sci. Data* **12**, 197–214. <https://doi.org/10.5194/essd-12-197-2020> (2020).
48. Zhao, J. *et al.* The variations of land surface phenology in Northeast China and its responses to climate change from 1982 to 2013. *Remote Sensing* **8**, 400. <https://doi.org/10.3390/rs8050400> (2016).
49. Reiners, P. *et al.* Validation of AVHRR land surface temperature with MODIS and in situ LST—A TIMELINE thematic processor. *Remote Sensing* **13**, 3473. <https://doi.org/10.3390/rs13173473> (2021).
50. Miao, L. *et al.* Unveiling the dynamics of sequential extreme precipitation-heatwave compounds in China. *NPJ Clim. Atmosph. Sci.* **7**, 67. <https://doi.org/10.1038/s41612-024-00613-5> (2024).
51. Du, Z., Zhao, J., Liu, X., Wu, Z. & Zhang, H. Recent asymmetric warming trends of daytime versus nighttime and their linkages with vegetation greenness in temperate China. *Environ. Sci. Pollut. Res.* **26**, 35717–35727. <https://doi.org/10.1007/s11356-019-06440-z> (2019).
52. Slayback, D. A., Pinzon, J. E., Los, S. O. & Tucker, C. J. Northern hemisphere photosynthetic trends 1982–99. *Glob. Change Biol.* **9**, 1–15. <https://doi.org/10.1046/j.1365-2486.2003.00507.x> (2003).
53. Zhou, Y. K., Fan, J. F. & Wang, X. Y. Assessment of varying changes of vegetation and the response to climatic factors using GIMMS NDVI3g on the Tibetan Plateau. *PLOS ONE* <https://doi.org/10.1371/journal.pone.0234848> (2020).
54. Fu, Y. *et al.* Climate and spring phenology effects on autumn phenology in the greater Khingan Mountains Northeastern China. *Remote Sensing* **10**, 449. <https://doi.org/10.3390/rs10030449> (2018).
55. Zuo, D. *et al.* Time-lag effects of climatic change and drought on vegetation dynamics in an alpine river basin of the Tibet Plateau China. *J. Hydrol.* **600**, 126532. <https://doi.org/10.1016/j.jhydrol.2021.126532> (2021).
56. Doan, Q.-V. *et al.* Causes for asymmetric warming of sub-diurnal temperature responding to global warming. *Geophys. Res. Lett.* **49**, e2022GL100029. <https://doi.org/10.1029/2022GL100029> (2022).
57. Zhang, Q., Kong, D., Shi, P., Singh, V. P. & Sun, P. Vegetation phenology on the Qinghai-Tibetan Plateau and its response to climate change (1982–2013). *Agric. Forest Meteorol.* **248**, 408–417. <https://doi.org/10.1016/j.agrformet.2017.10.026> (2018).
58. Hijmans, R. J., Cameron, S. E., Parra, J. L., Jones, P. G. & Jarvis, A. Very high resolution interpolated climate surfaces for global land areas. *Int. J. Climatol.* **25**, 1965–1978. <https://doi.org/10.1002/joc.1276> (2005).

59. Wang, X. *et al.* No trends in spring and autumn phenology during the global warming hiatus. *Nat. Commun.* **10**, 2389. <https://doi.org/10.1038/s41467-019-10235-8> (2019).
60. Ren, S., Li, Y. & Peichl, M. Diverse effects of climate at different times on grassland phenology in mid-latitude of the Northern Hemisphere. *Ecol. Indicat.* **113**, 106260. <https://doi.org/10.1016/j.ecolind.2020.106260> (2020).
61. Li, Q. *et al.* Remote sensing of seasonal climatic constraints on leaf phenology across pantropical evergreen forest biome. *Earth's Future* **9**, e2021EF002160. <https://doi.org/10.1029/2021EF002160> (2021).
62. Peaucelle, M. *et al.* Spatial variance of spring phenology in temperate deciduous forests is constrained by background climatic conditions. *Nat. Commun.* **10**, 5388. <https://doi.org/10.1038/s41467-019-13365-1> (2019).
63. Wang, J. Y. A critique of the heat unit approach to plant response studies. *Ecology* **41**, 785–790. <https://doi.org/10.2307/1931815> (1960).
64. Deng, G. *et al.* Asymmetric effects of daytime and nighttime warming on boreal forest spring phenology. *Remote Sensing* **11**, 1651. <https://doi.org/10.3390/rs11141651> (2019).
65. Lian, X. *et al.* Seasonal biological carryover dominates northern vegetation growth. *Nat. Commun.* <https://doi.org/10.1038/s41467-021-21223-2> (2021).
66. Renner, S. S. & Zohner, C. M. The occurrence of red and yellow autumn leaves explained by regional differences in insolation and temperature. *New Phytologist* **224**, 1464–1471. <https://doi.org/10.1111/nph.15900> (2019).
67. Zani, D., Crowther, T. W., Mo, L., Renner, S. S. & Zohner, C. M. Increased growing-season productivity drives earlier autumn leaf senescence in temperate trees. *Science* **370**, 1066–1071. <https://doi.org/10.1126/science.abd8911> (2020).
68. Wu, Z. *et al.* Atmospheric brightening counteracts warming-induced delays in autumn phenology of temperate trees in Europe. *Glob. Ecol. Biogeograph.* **30**, 2477–2487. <https://doi.org/10.1111/geb.13404> (2021).
69. Li, C. *et al.* Responses of vegetation spring phenology to climatic factors in Xinjiang China. *Ecol. Indicat.* **124**, 107286. <https://doi.org/10.1016/j.ecolind.2020.107286> (2021).
70. Che, M. *et al.* Spatial and temporal variations in the end date of the vegetation growing season throughout the Qinghai-Tibetan Plateau from 1982 to 2011. *Agric. Forest Meteorol.* **189–190**, 81–90. <https://doi.org/10.1016/j.agrformet.2014.01.004> (2014).
71. Shi, C. *et al.* Climate warming alters nitrogen dynamics and total non-structural carbohydrate accumulations of perennial herbs of distinctive functional groups during the plant senescence in autumn in an alpine meadow of the Tibetan Plateau China. *Agric. Forest Meteorol.* **200**, 21–29. <https://doi.org/10.1016/j.agrformet.2014.09.006> (2015).
72. Yang, Z. *et al.* Asymmetric responses of the end of growing season to daily maximum and minimum temperatures on the Tibetan plateau. *J. Geophys. Res. Atmosph.* **122**, 13278–13287. <https://doi.org/10.1002/2017jd027318> (2017).
73. Du, J. *et al.* Daily minimum temperature and precipitation control on spring phenology in arid-mountain ecosystems in China. *Int. J. Climatol.* **40**, 2568–2579. <https://doi.org/10.1002/joc.6351> (2020).

Acknowledgements

This work was supported by Hainan Provincial Natural Science Foundation of China [grant number 623QY621] and the Natural Science Foundation of Fujian Province [grant number 2021J01627].

Author contributions

Conceptualization, Q.W., H.C. and F.X.; validation, V.B., Q.W. and F.X.; formal analysis, H.C., F.X. and Q.W.; Methodology, H.C. R.Z. and Q.W.; investigation, F.X. R.Z., and W.X.; data curation, F.X. R.Z., and W.X.; writing—original draft preparation, F.X.; writing—review and editing, H.C., V.B. and Q.W.; visualization, W.X.; supervision, V.B., P.G. and Q.W.; funding acquisition, Q.W., P.G. All authors contributed to finalize the manuscript.

Competing interests

The authors declare no competing interests.

Additional information

Supplementary Information The online version contains supplementary material available at <https://doi.org/10.1038/s41598-024-59336-5>.

Correspondence and requests for materials should be addressed to Q.W. or P.G.

Reprints and permissions information is available at www.nature.com/reprints.

Publisher's note Springer Nature remains neutral with regard to jurisdictional claims in published maps and institutional affiliations.



Open Access This article is licensed under a Creative Commons Attribution 4.0 International License, which permits use, sharing, adaptation, distribution and reproduction in any medium or format, as long as you give appropriate credit to the original author(s) and the source, provide a link to the Creative Commons licence, and indicate if changes were made. The images or other third party material in this article are included in the article's Creative Commons licence, unless indicated otherwise in a credit line to the material. If material is not included in the article's Creative Commons licence and your intended use is not permitted by statutory regulation or exceeds the permitted use, you will need to obtain permission directly from the copyright holder. To view a copy of this licence, visit <http://creativecommons.org/licenses/by/4.0/>.

© The Author(s) 2024